

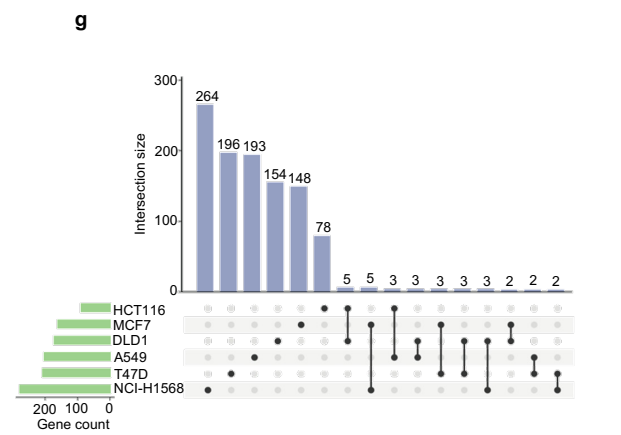
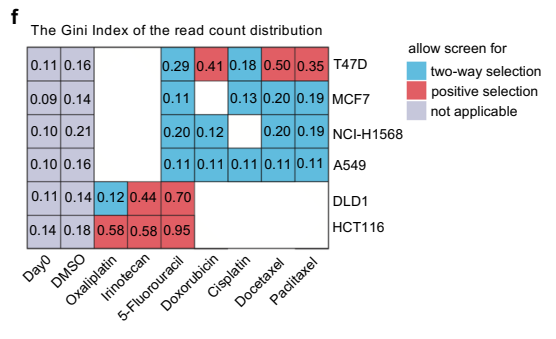
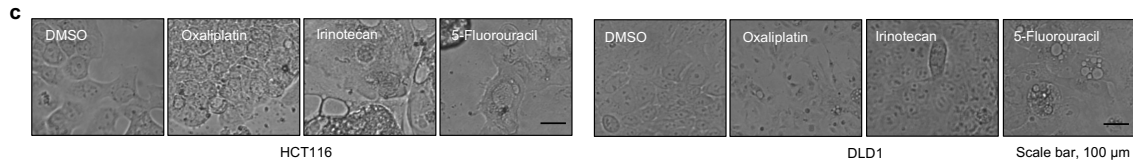
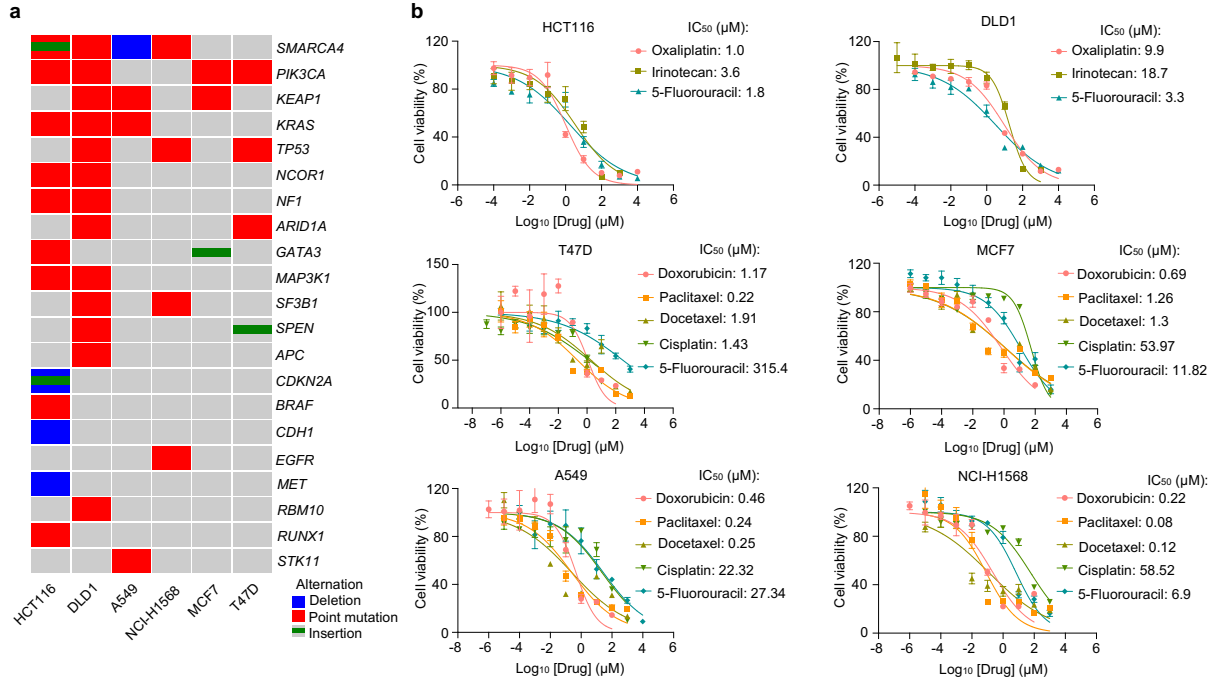
SUPPLEMENTARY INFORMATION

CRISPR screens reveal convergent targeting strategies against evolutionarily distinct chemoresistance in cancer

Supplementary Information associated with this article include:

Supplementary Figs. 1-19

Supplementary Data 1-6 (attached datasets)



Supplementary Fig. 1 Chemogenomic CRISPR screens.

a, Mutational profile of typical cancer-related genes for indicated cancer cell lines.

b, Cell viability assays to determine IC_{50} values of indicated drugs for corresponding cell lines. Mean \pm SD with $n \geq 3$ biological replicates.

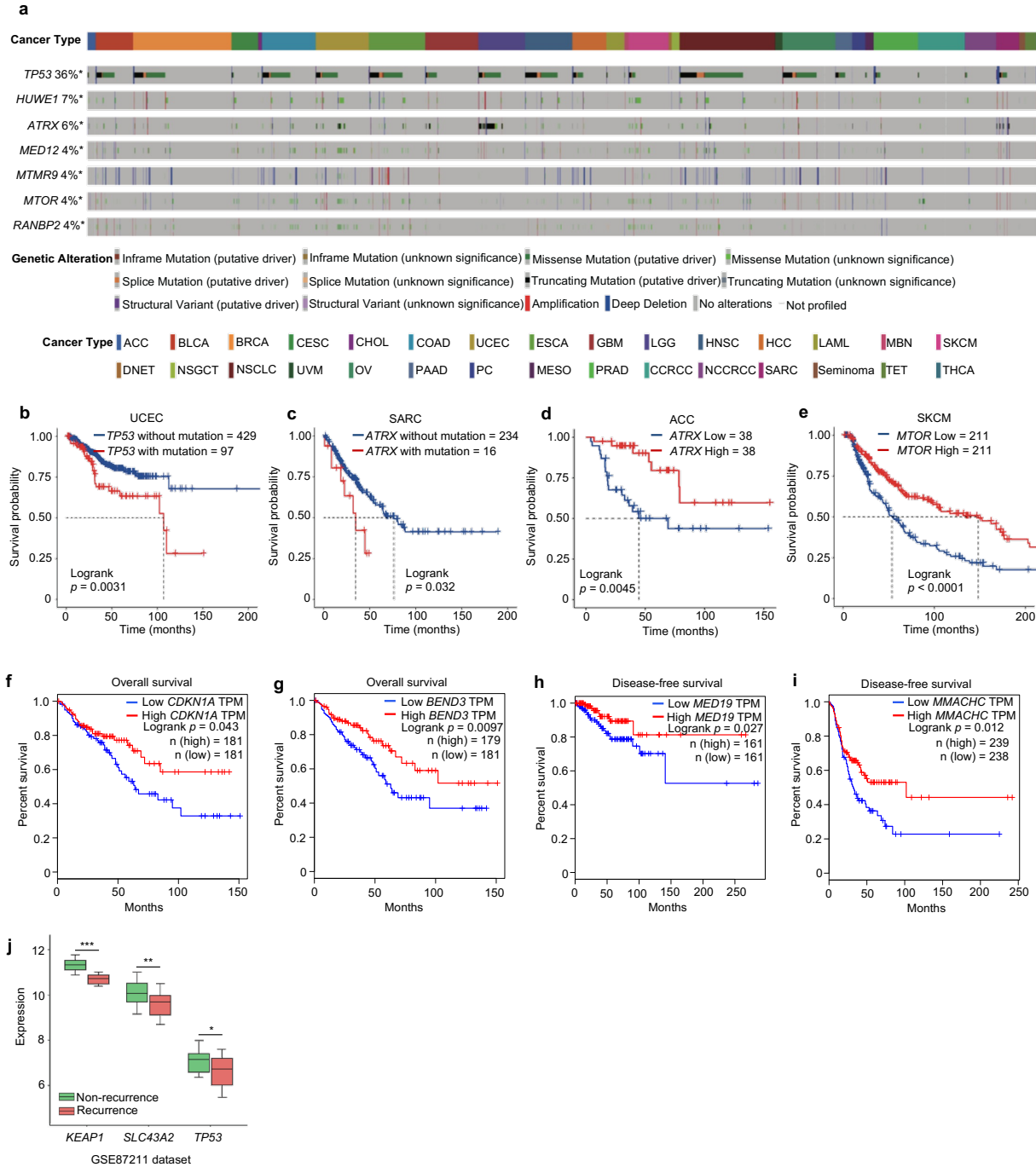
c, Cell morphology of HCT116 and DLD1 cells after chemogenomic screens before cell sample collection. Scale bar, 100 μ m.

d, Violin plot showing the RRA score for all the genes or essential genes in the screens (DMSO condition for each cell line). Wilcoxon test, all p -value $< 2.2e-16$, *** $p < 0.001$.

e, House-keeping functional terms are enriched among top 500 negatively selected genes in each screen (DMSO condition for each cell line). Unpaired two-sided t test for p value with Benjamini-Hochberg (BH) adjustment.

f, The Gini Index showing the distribution of sgRNA read counts for each screen sample. A smaller value indicates more evenness of the count distribution. Significant distortion of sgRNA counts (Gini Index > 0.3) in the screen makes it inappropriate to analyze negatively selected genes.

g, Overlap of chemoresistance genes for the six cell lines.



Supplementary Fig. 2 | Identification and analysis of chemosensitizer genes.

a, Overview of genetic alterations of representative chemoresistance genes in TCGA.

b, Overall survival analysis of Uterine Corpus Endometrial Carcinoma (UCEC) patients with *TP53* mutational status.

c, Overall survival analysis of Sarcoma (SARC) patients with *ATRX* mutational status.

d, Overall survival analysis of Adrenocortical carcinoma (ACC) patients with *ATRX* expression status.

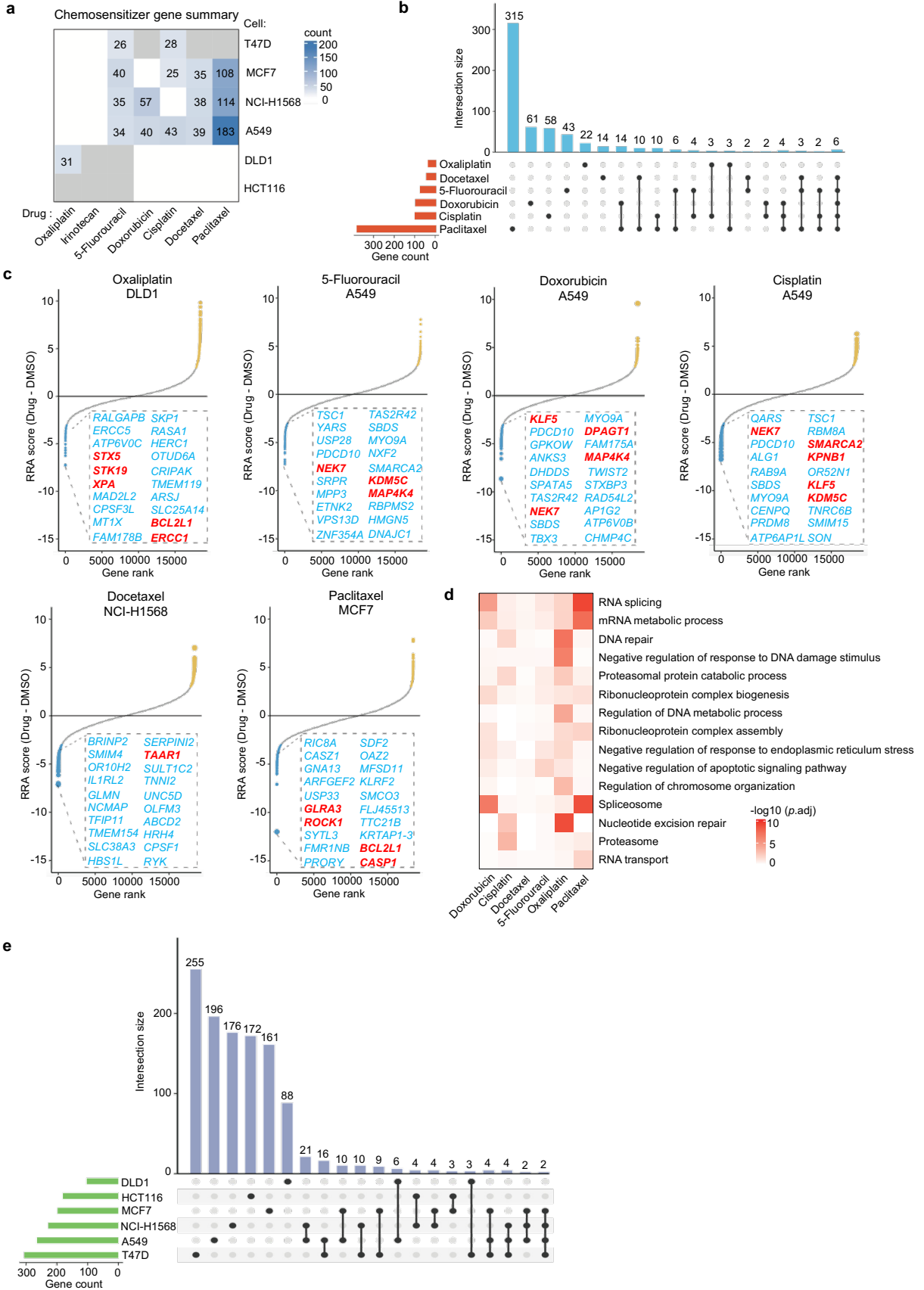
e, Overall survival analysis of Skin Cutaneous Melanoma (SKCM) patients with *MTOR* expression status.

f-g, Overall survival analysis of colorectal cancer patients using COADREAD data from TCGA with *CDKN1A* (**f**) or *BEND3* (**g**) expression levels.

h, Disease-free survival analysis of breast cancer patients using BRCA data from TCGA with *MED19* expression levels.

i, Disease-free survival analysis of lung cancer patients using LUAD data from TCGA with *MMACHC* expression levels.

j, Expression levels of *KEAP1* ($p < 1e-10$), *TP53* ($p = 0.0014$), and *SLC43A2* ($p = 0.036$) in recurrent or non-recurrent tumors from RNA-seq data of a colorectal cancer patient cohort treated with oxaliplatin. 92 out of 203 patients in this cohort received oxaliplatin treatment and 20 patients showed recurrence after the treatment. Unpaired two-sided t test.



Supplementary Fig. 3 | Identification and analysis of chemosensitizer genes.

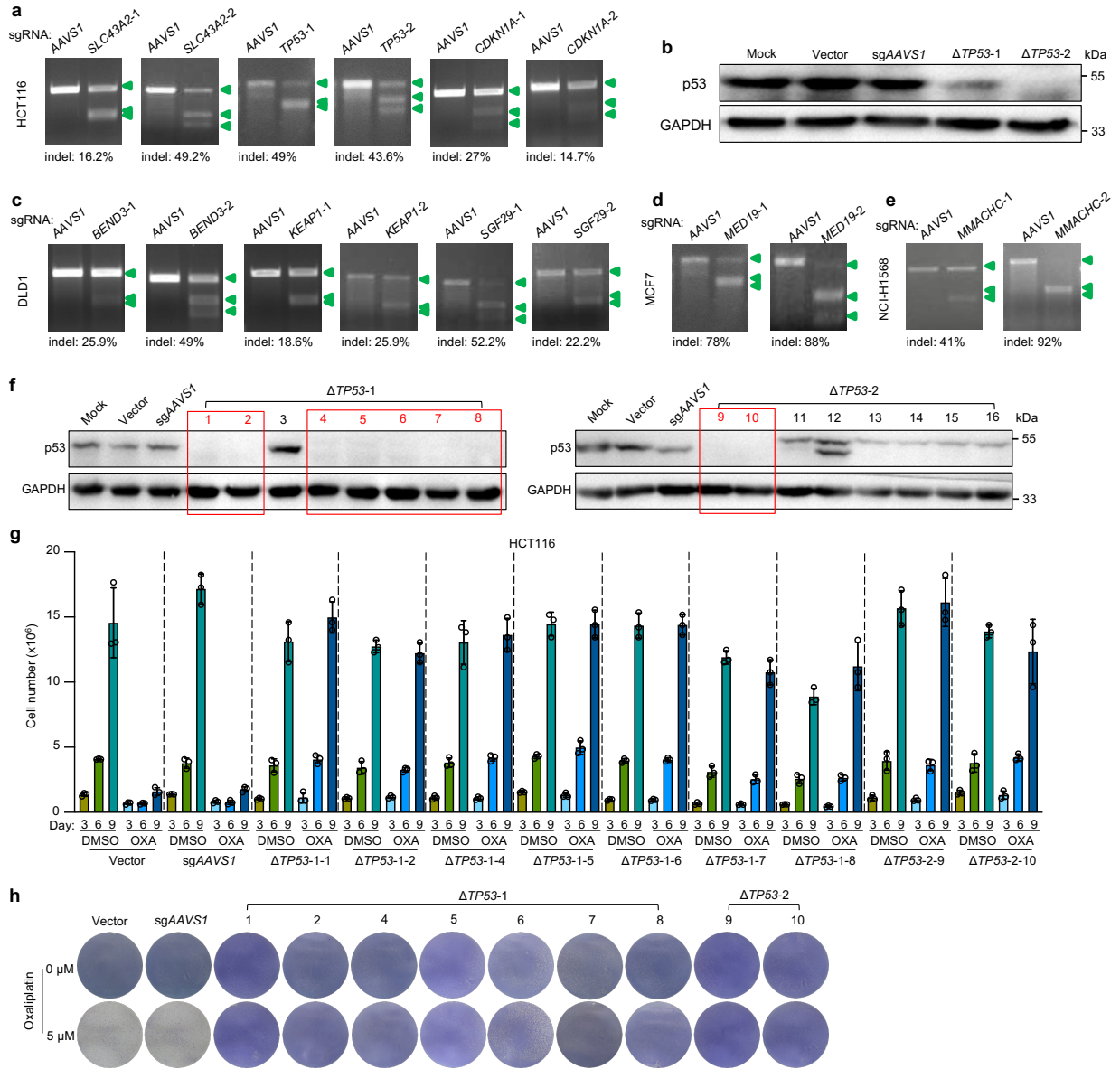
a, The number of chemosensitizer genes identified from each indicated screen.

b, Overlap of chemosensitizer genes for each chemotherapy drug.

c, Top chemosensitizer genes from representative screens for each chemotherapy drug. Genes with available targeted inhibitors are highlighted in red bold font.

d, Enriched functional terms from KEGG and GO for chemosensitizer genes of indicated chemotherapy drugs. Unpaired two-sided t test for p value with Benjamini-Hochberg (BH) adjustment.

e, Overlap of chemosensitizer genes for the six cell lines.



Supplementary Fig. 4 | CRISPR-mediated knockout of individual chemoresistance genes.

a, Indel assay based on T7 endonuclease I showing the effectiveness of indicated sgRNAs to generate indels at target gene loci in HCT116 cells.

b, Immunoblot of p53 for control and *TP53* knockout HCT116 cells.

c, Indel assay showing the effectiveness of indicated sgRNAs at target gene loci in DLD1 cells.

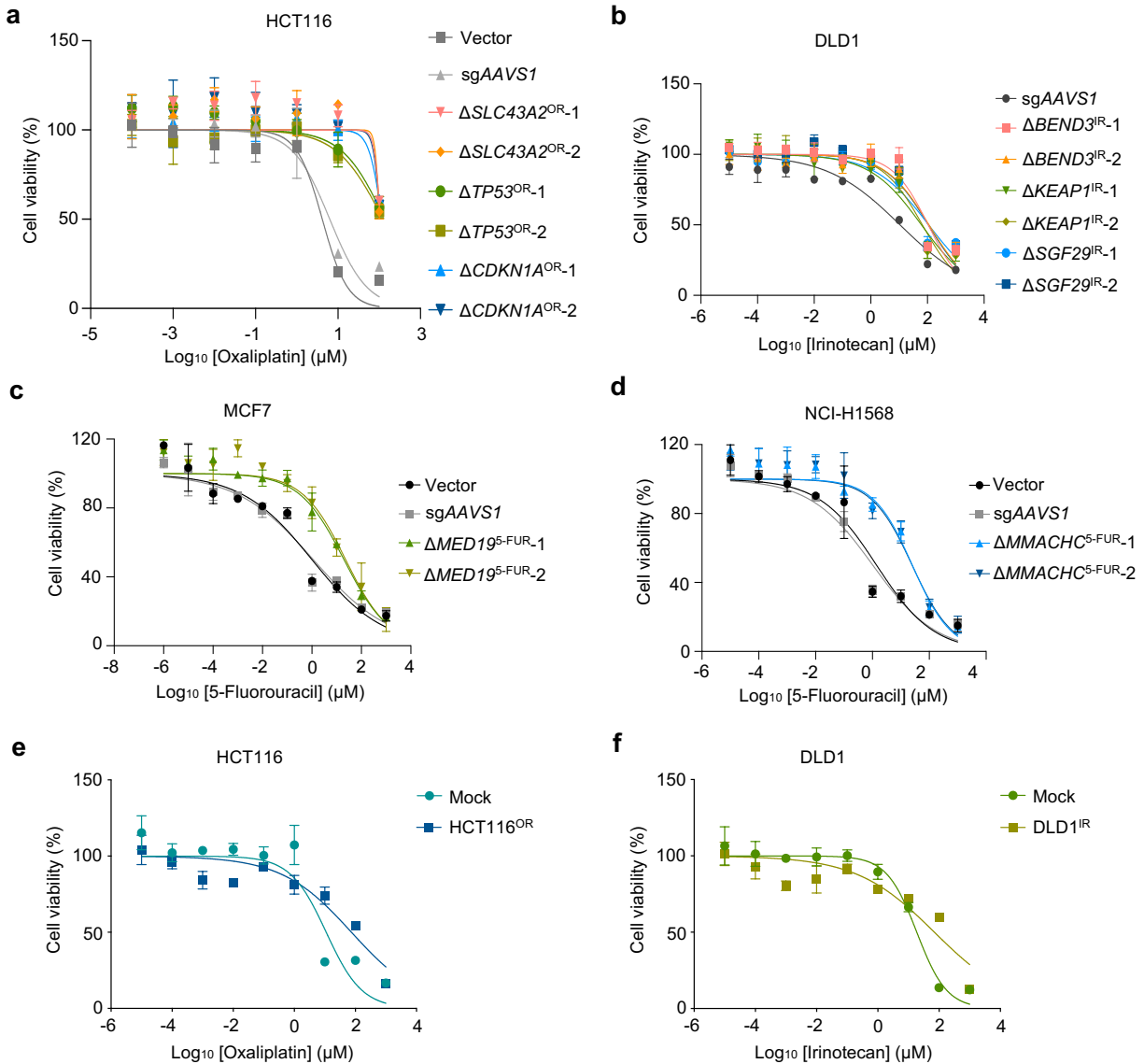
d, Indel assay based on T7 endonuclease I showing the effectiveness of indicated sgRNAs to generate indels at target gene loci in MCF7 cells.

e, Indel assay showing the effectiveness of indicated sgRNAs at target gene loci in NCI-H1568 cells.

f, Immunoblot of p53 for different single clones of *TP53* knockout cells. The clones with complete p53 knockout are marked in red.

g, Cell number quantification using a hemocytometer for indicated cells treated with DMSO or oxaliplatin. OXA, oxaliplatin. Mean \pm SD with n = 3 biological replicates.

h, Crystal violet staining of indicated cells treated with oxaliplatin.



Supplementary Fig. 5 | Cell viability assay for determining IC₅₀ of the drugs.

a, Cell viability assay (MTT method) of different sensitive (Vector-without sgRNA, sgAAVS1-expressing sgRNA targeting *AAVS1* locus) and resistant HCT116 cell lines (established by indicated gene knockout and oxaliplatin selection) in response to oxaliplatin. OR, oxaliplatin resistance. -1 and -2 indicate different sgRNAs for individual gene knockout. Mean \pm SD with n = 3 biological replicates.

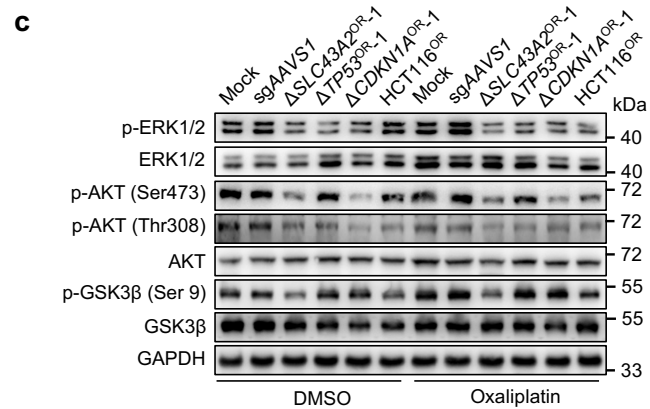
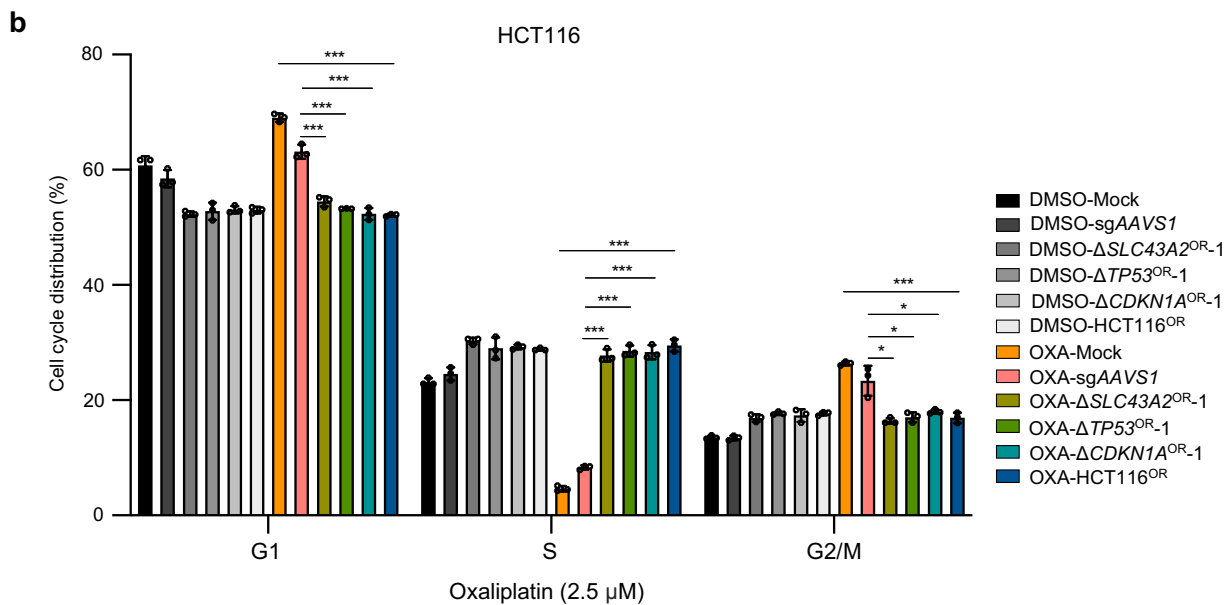
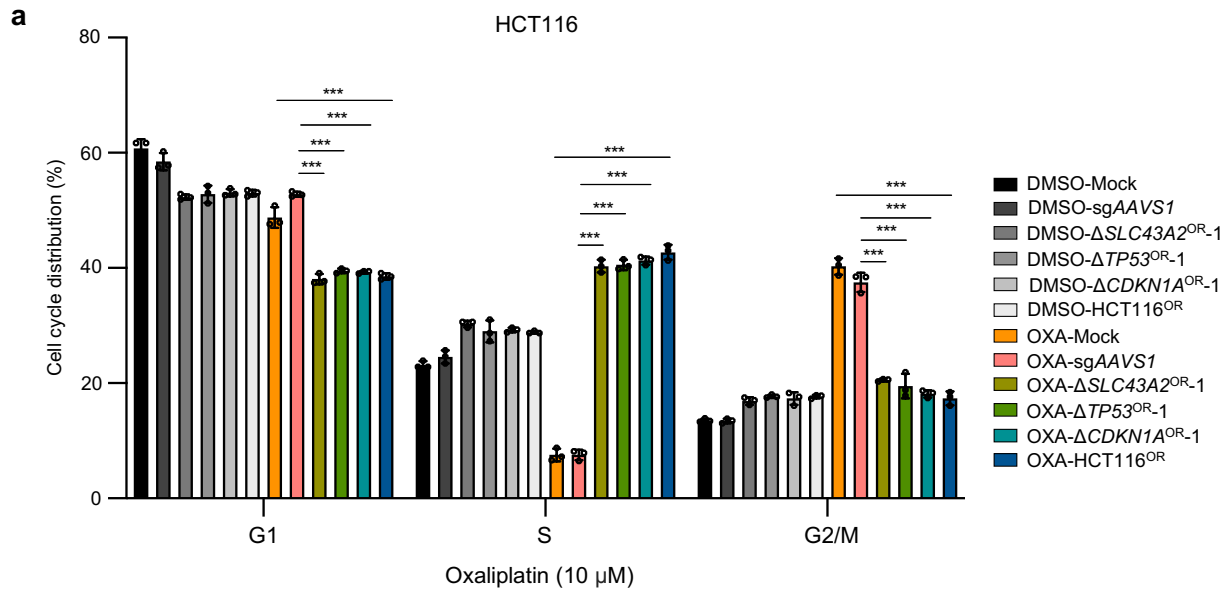
b, Cell viability assays evaluating the response of different irinotecan-resistant DLD1 cell lines (established by individual gene knockout and irinotecan selection) to irinotecan. IR, irinotecan resistance. Mean \pm SD with n = 3 biological replicates.

c, Cell viability assay of different sensitive and resistant MCF7 cell lines (established by *MED19* knockout and 5-Fluorouracil selection) in response to 5-Fluorouracil. 5-FUR, 5-Fluorouracil resistance. Mean \pm SD with n = 3 biological replicates.

d, Cell viability assay of different sensitive and resistant NCI-H1568 cell lines (established by *MMACHC* knockout and 5-Fluorouracil selection) in response to 5-Fluorouracil. Mean \pm SD with n = 3 biological replicates.

e, MTT-based cell viability assay for parental and HCT116^{OR} cells. Mean \pm SD with n = 3 biological replicates.

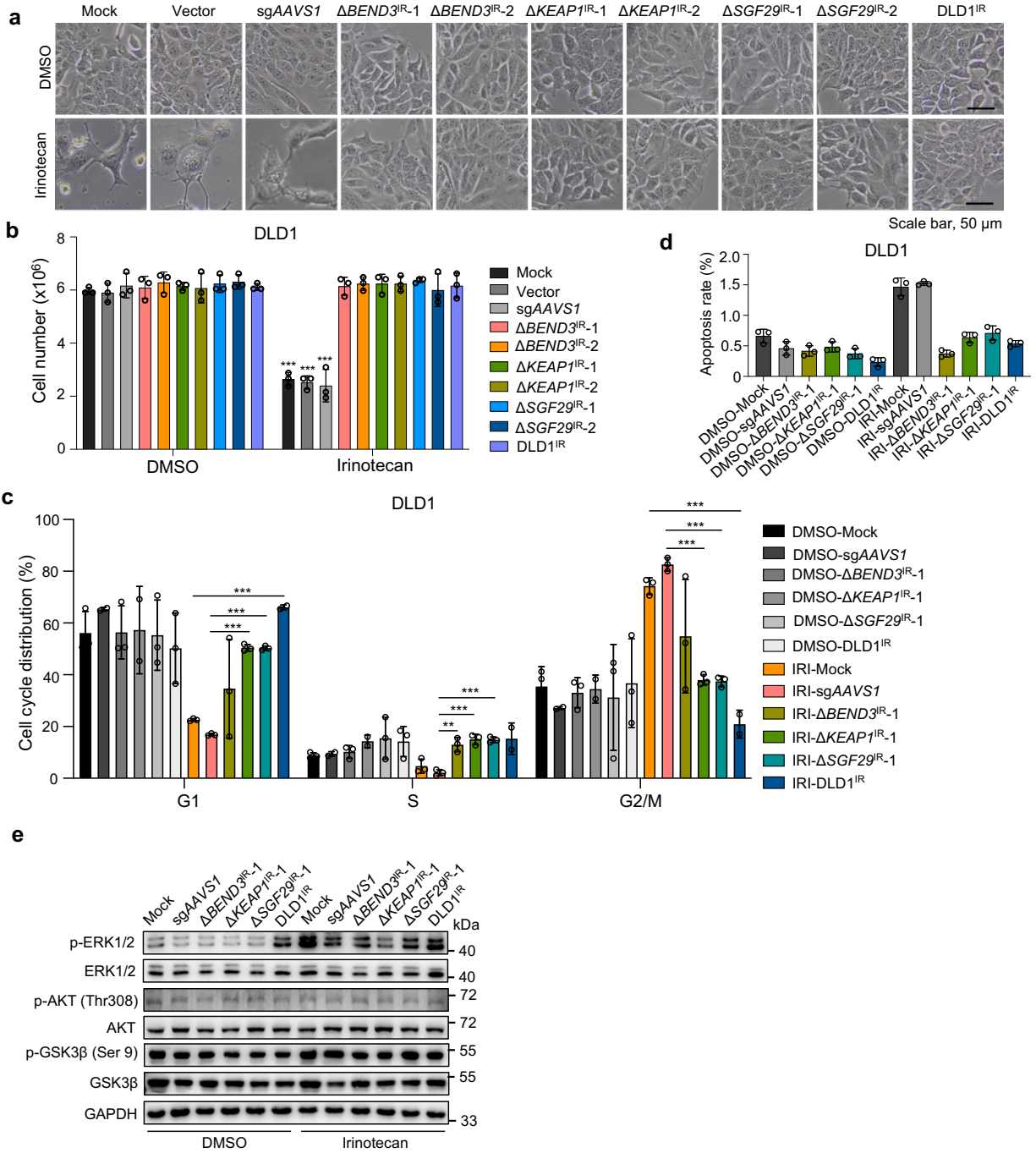
f, MTT-based cell viability assay for parental and DLD1^{IR} cells. Mean \pm SD with n = 3 biological replicates.



Supplementary Fig. 6 | Additional characterization of oxaliplatin-resistant cells.

a-b, Cell cycle analysis by propidium iodide (PI) staining of indicated cell lines in the absence or presence of 10 μM (**a**) or 2.5 μM (**b**) oxaliplatin for 48 h. OXA, oxaliplatin. Mean \pm SD with $n = 3$ biological replicates. Unpaired two-sided t test, $*p < 0.05$ and $***p < 0.001$.

c, Immunoblot analysis of indicated proteins for multiple oxaliplatin-sensitive or -resistant HCT116 cell lines in the absence or presence of 5 μM oxaliplatin for 72 h.



Supplementary Fig. 7 | Cellular and molecular features of irinotecan-resistant cells.

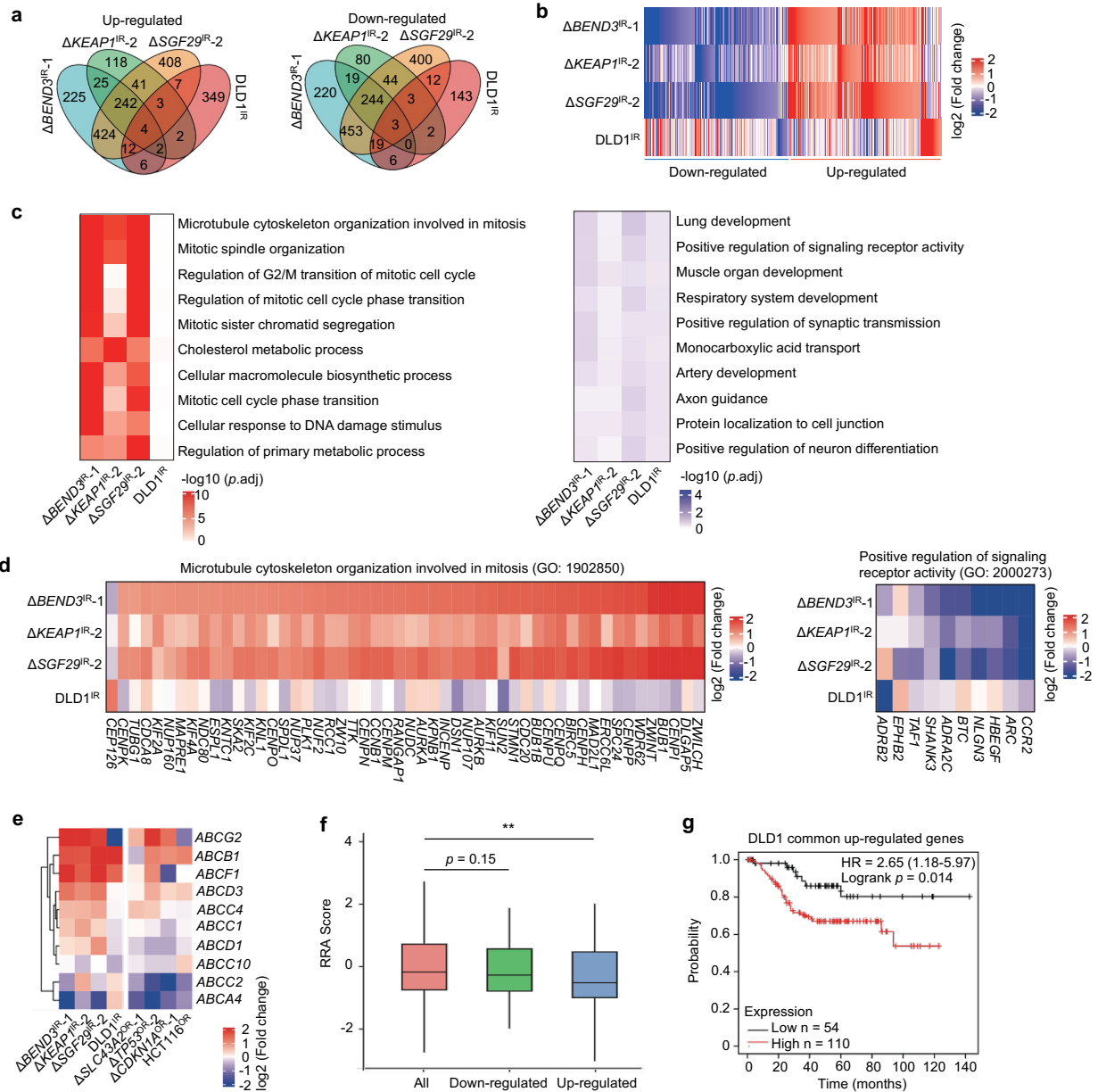
a, Cell morphology of multiple irinotecan-sensitive (Mock, Vector and *sgAAVS1* groups) and -resistant cell lines in the absence or presence of irinotecan. Scale bar, 50 μm .

b, Cell number quantification of indicated irinotecan-sensitive and -resistant cell lines after 7 days of irinotecan treatment. Mean \pm SD with $n = 3$ biological replicates. Unpaired two-sided t test (irinotecan vs. DMSO), *** $p < 0.001$.

c, Cell cycle analysis by PI staining of indicated cell lines in the absence or presence of 10 μ M irinotecan for 24 h. IRI, irinotecan. Mean \pm SD with n = 3 biological replicates. Unpaired two-sided t test, ** $p < 0.01$ and *** $p < 0.001$.

d, Apoptosis analysis by PI and Hoechst staining of indicated cell lines in the absence or presence of 10 μ M irinotecan for four days. Mean \pm SD with n = 3 biological replicates.

e, Immunoblot analysis of indicated proteins for multiple irinotecan-sensitive or -resistant DLD1 cell lines in the absence or presence of 10 μ M irinotecan for 72 h.



Supplementary Fig. 8 | Gene expression profiles of irinotecan-resistant cells.

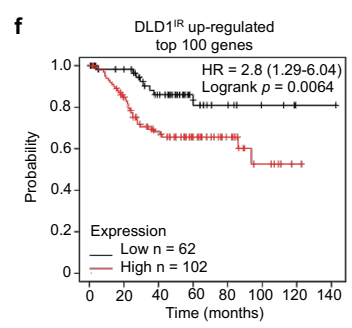
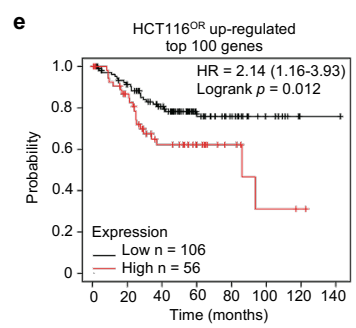
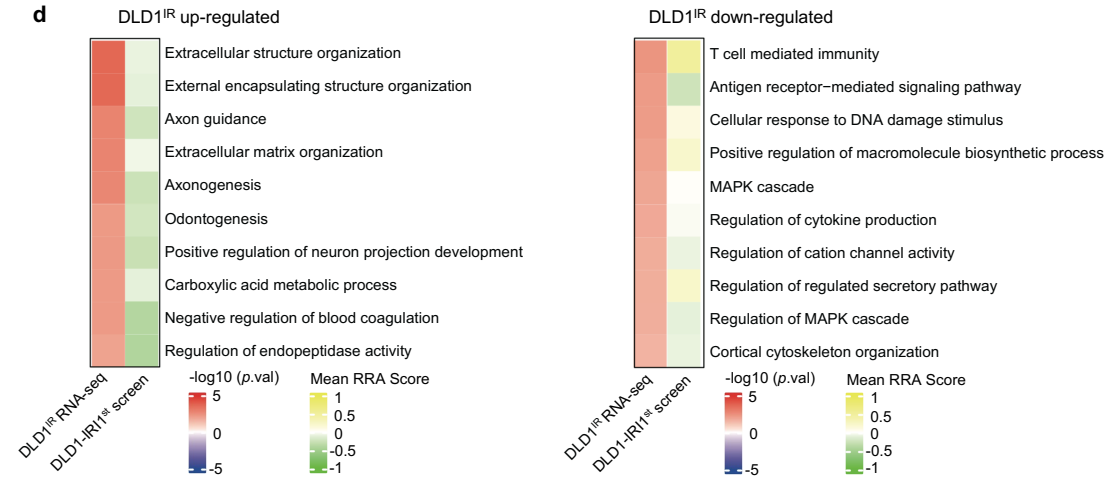
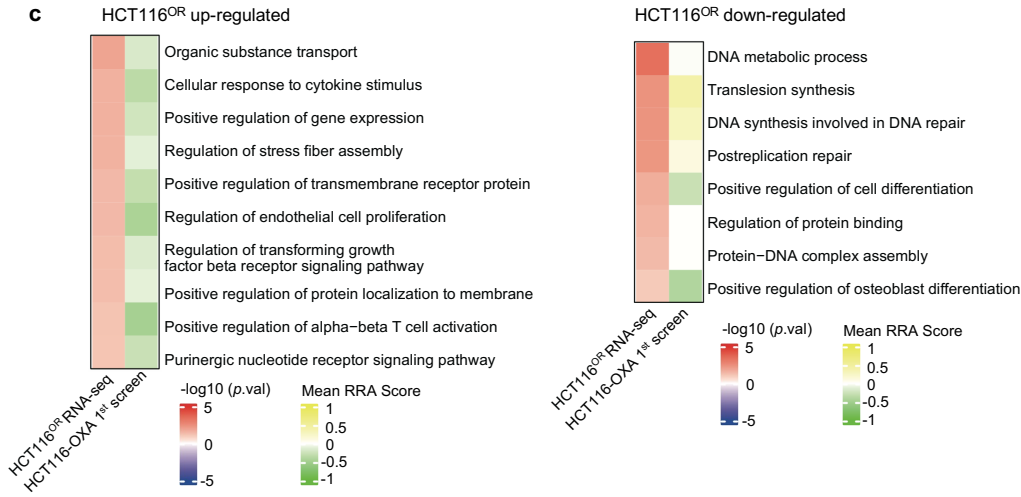
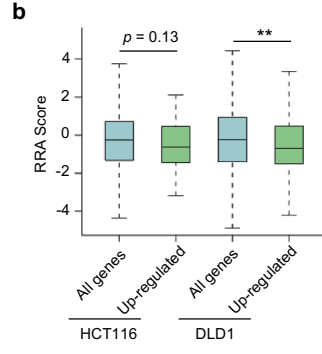
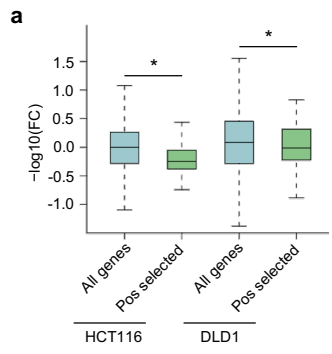
a, Venn diagram of differentially expressed genes ($\Delta BEND3^{IR-1}$, $\Delta KEAP1^{IR-2}$ or $\Delta SGF29^{IR-2}$ vs. sgAAVSI; DLD1^{IR} vs. untreated Mock) in four indicated irinotecan-resistant DLD1 cell lines determined by RNA-seq analysis.

b, Heatmap showing differentially expressed genes in four indicated irinotecan-resistant DLD1 cell lines. Unpaired two-sided t test for p value with Benjamini-Hochberg (BH) adjustment.

c, Functional enrichment analysis showing the prominently enriched terms among up-regulated (left) or down-regulated (right) genes in four DLD1 irinotecan-resistant cell lines relative to -sensitive control cells.

d, Highlight of individual genes within indicated functional terms across the four irinotecan-resistant cell lines.

- e**, Expression change of typical ABC transporter genes associated with multidrug resistance.
- f**, RRA Score for commonly up- or down-regulated genes in $\Delta BEND3^{IR}$, $\Delta KEAP1^{IR}$ and $\Delta SGF29^{IR}$ resistance models during DLD1-irinotecan chemoresistance screen. Unpaired two-sided t test, $p = 0.008$.
- g**, Survival analysis of commonly up-regulated genes in $\Delta BEND3^{IR}$, $\Delta KEAP1^{IR}$ and $\Delta SGF29^{IR}$ resistance models in a colorectal cancer patient cohort (GSE17538).



Supplementary Fig. 9 | Relationship between chemoresistant genes from CRISPR screen and differential genes from RNA-seq in HCT116^{OR} or DLD1^{IR} resistant models.

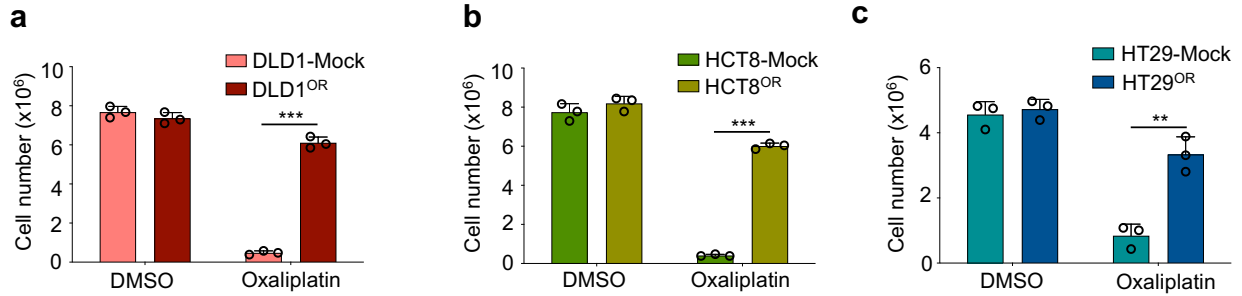
a, The expression status of positively selected gene hits during corresponding chemoresistance CRISPR screen in RNA-seq data of HCT116^{OR} ($p = 0.033$) and DLD1^{IR} ($p = 0.014$) resistance models. Unpaired two-sided t test.

b, The RRA score of significantly up-regulated genes in HCT116^{OR} ($p = 0.131$) and DLD1^{IR} ($p = 0.004$) resistance models during HCT116-oxaliplatin or DLD1-irinotecan chemoresistant screen. Unpaired two-sided t test.

c, The prominently enriched functional terms for up-regulated or down-regulated genes in HCT116^{OR} resistance model and their mean RRA scores for the genes in corresponding terms during HCT116-oxaliplatin chemoresistance screen. Unpaired two-sided t test for p value with Benjamini-Hochberg (BH) adjustment.

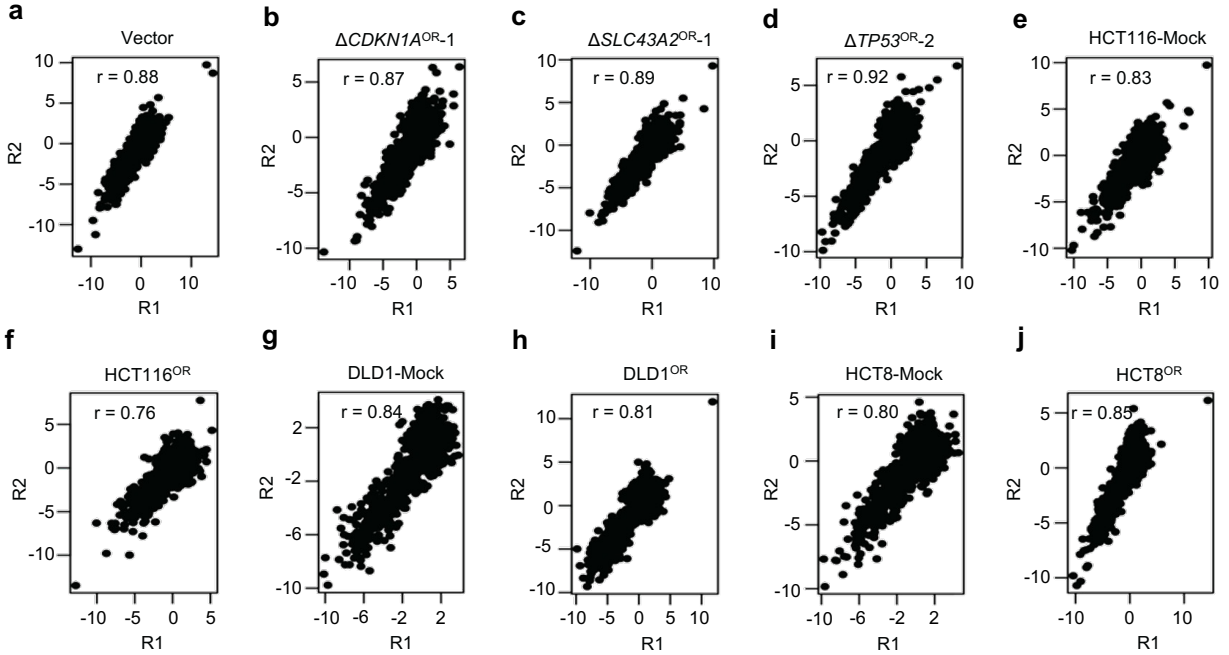
d, The prominently enriched functional terms for up-regulated or down-regulated genes in DLD1^{IR} resistance model and their mean RRA scores for the genes in corresponding terms during DLD1-irinotecan chemoresistance screen. Unpaired two-sided t test for p value with Benjamini-Hochberg (BH) adjustment.

e-f, Survival analysis of top 100 up-regulated genes in HCT116^{OR} (**e**) or DLD1^{IR} (**f**) resistance models in a colorectal cancer patient cohort (GSE17538).



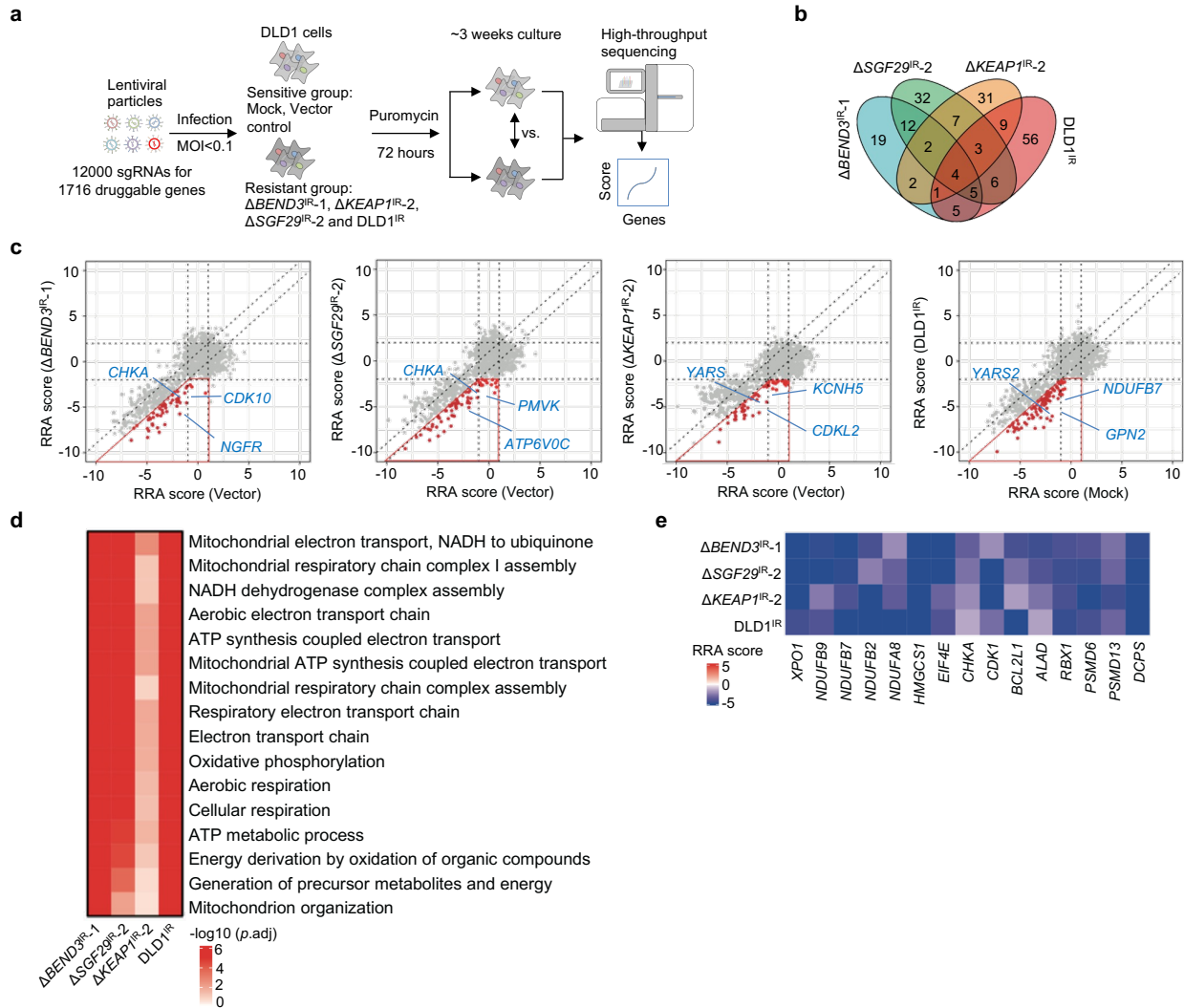
Supplementary Fig. 10 | Establishment of additional oxaliplatin-resistant lines with various genetic backgrounds by traditional drug pulsing and clonal selection method.

a-c, Cell growth response to oxaliplatin for indicated parental cells and resistant cells established by “randomly” clonal selection with gradual increase of oxaliplatin treatment. Cell number was quantified after treatment of DLD1 cells with 80 μ M oxaliplatin for 7 days (**a**), HCT8 cells with 50 μ M oxaliplatin for 7 days (**b**) and HT29 cells with 35 μ M oxaliplatin for 10 days (**c**), respectively. Mean \pm SD with $n = 3$ biological replicates. Unpaired two-sided t test, $**p < 0.01$ and $***p < 0.001$.



Supplementary Fig. 11 | Replicate correlation for indicated second-round CRISPR screen samples.

a-j, Correlation of RRA scores between the two biological replicates (R1 and R2) across all the indicated conditions during second-round druggable CRISPR screens against oxaliplatin resistance.



Supplementary Fig. 12 | Interrogation of druggable targets against irinotecan resistance by second-round CRISPR screens.

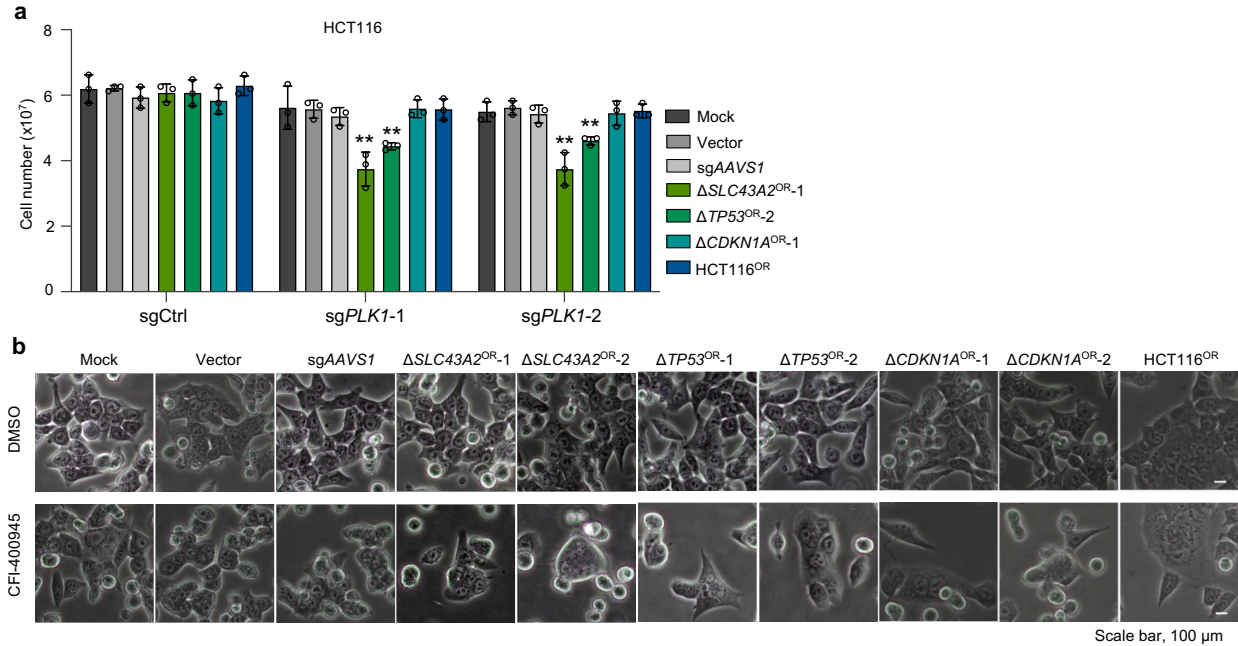
a, Workflow of identification of potential targets against irinotecan resistance using druggable gene CRISPR knockout screens.

b, Venn diagram of preferably druggable gene hits ($\Delta BEND3^{IR-1}$, $\Delta KEAP1^{IR-2}$ or $\Delta SGF29^{IR-2}$ vs. Vector; $DLD1^{IR}$ vs. untreated Mock) in four irinotecan-resistant DLD1 cell lines by second-round CRISPR screens.

c, The RRA scores of all the tested genes for irinotecan-sensitive control or -resistance cells in each comparison. The genes in red box are preferential targets against resistance. Several representative genes are highlighted.

d, The prominently enriched functional terms for druggable gene sets against irinotecan identified from second-round CRISPR screens in four resistant cell lines. Unpaired two-sided t test for p value with Benjamini-Hochberg (BH) adjustment.

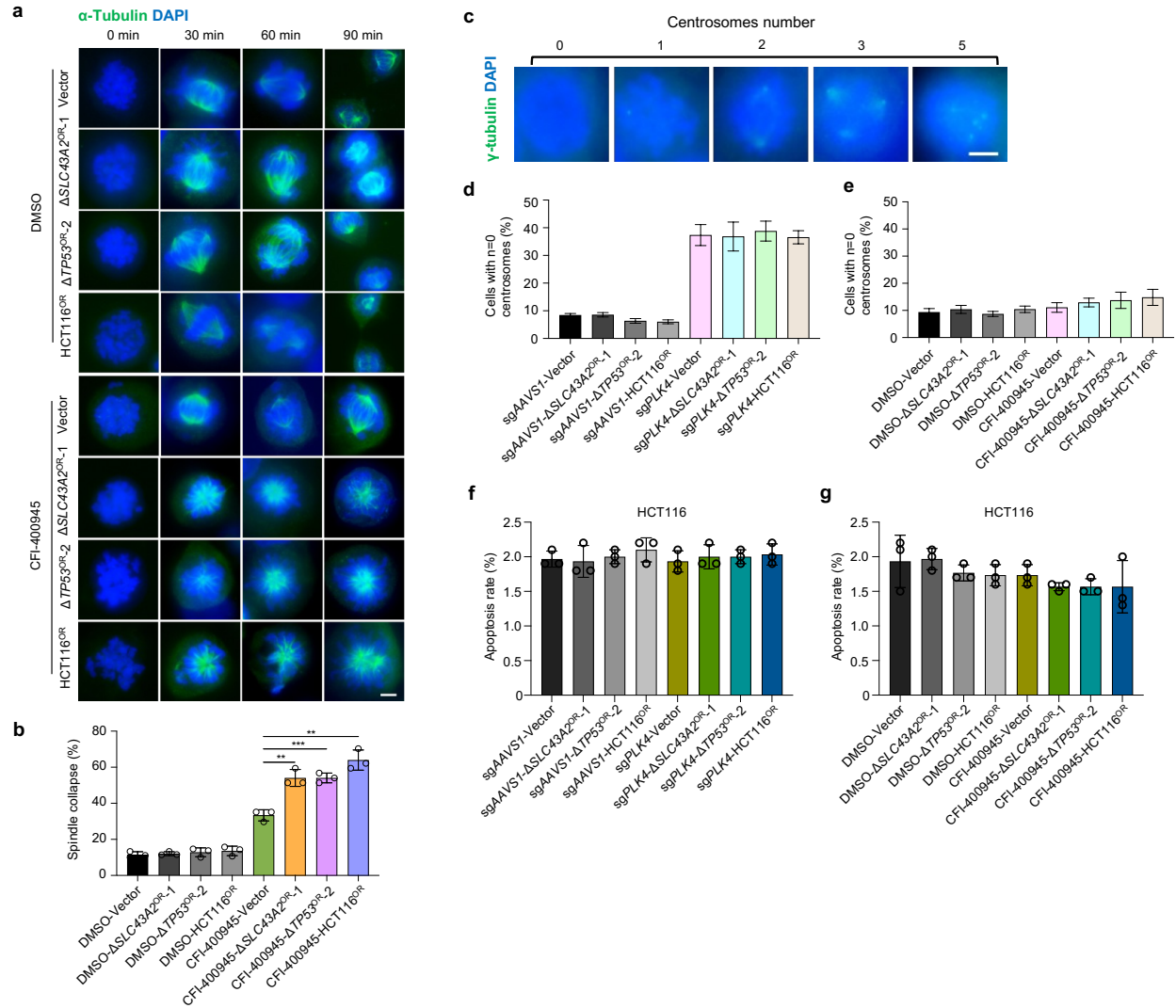
e, Heatmap showing the RRA scores for the top consensus druggable targets across all the four irinotecan-resistant cell lines.



Supplementary Fig. 13 | Cell growth effect of *PLK1* knockout and cellular morphology upon *PLK4* inhibitor treatment for oxaliplatin-resistant cells.

a, Cell growth effect of *PLK1* knockout by two independent sgRNAs in oxaliplatin-sensitive or -resistant cell lines. Mean \pm SD with $n = 3$ biological replicates. Unpaired two-sided t test ($\Delta SLC43A2^{OR}$, $\Delta TP53^{OR}$ or $\Delta CDKN1A^{OR}$ vs. sgAAVS1; HCT116^{OR} vs. Mock), $**p < 0.01$.

b, Cell morphology of multiple oxaliplatin-sensitive (Mock, Vector and sgAAVS1 groups) and -resistant cell lines in the absence or presence of 12 nM CFI-400945 for one week. Scale bar, 100 μ m.



Supplementary Fig. 14 | Targeting PLK4 in oxaliplatin-resistant cells.

a, Treatment with CFI-400945 results in spindle collapse, folding and slippage in oxaliplatin-resistant cells. Scale bar, 5 μ m.

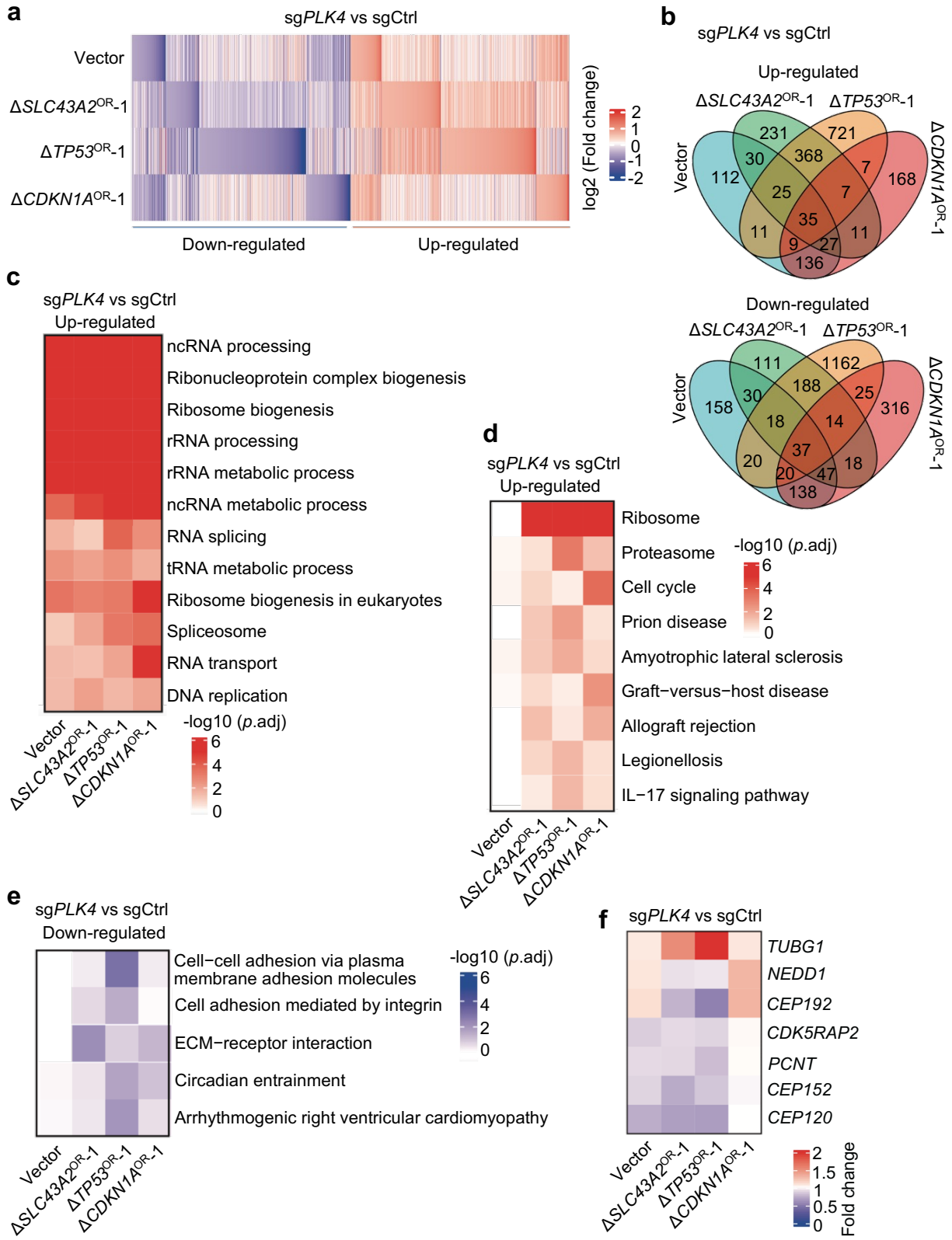
b, Quantification of spindle collapse for **(a)**. Mean \pm SD with n = 3 biological replicates, 100-200 cells were analyzed per independent experiment. Unpaired two-sided t test, * $p < 0.05$ and ** $p < 0.01$.

c, Representative images for centrosome quantification by γ -tubulin staining.

d-e, Distribution of cell populations with zero centrosome number before or after *PLK4* knockout **(d)** or CFI-400945 treatment **(e)** for oxaliplatin-sensitive and -resistant cells. Mean \pm SD with n = 3 biological replicates, 100-200 cells were analyzed per independent experiment. Unpaired two-sided t test, * $p < 0.05$ and ** $p < 0.01$.

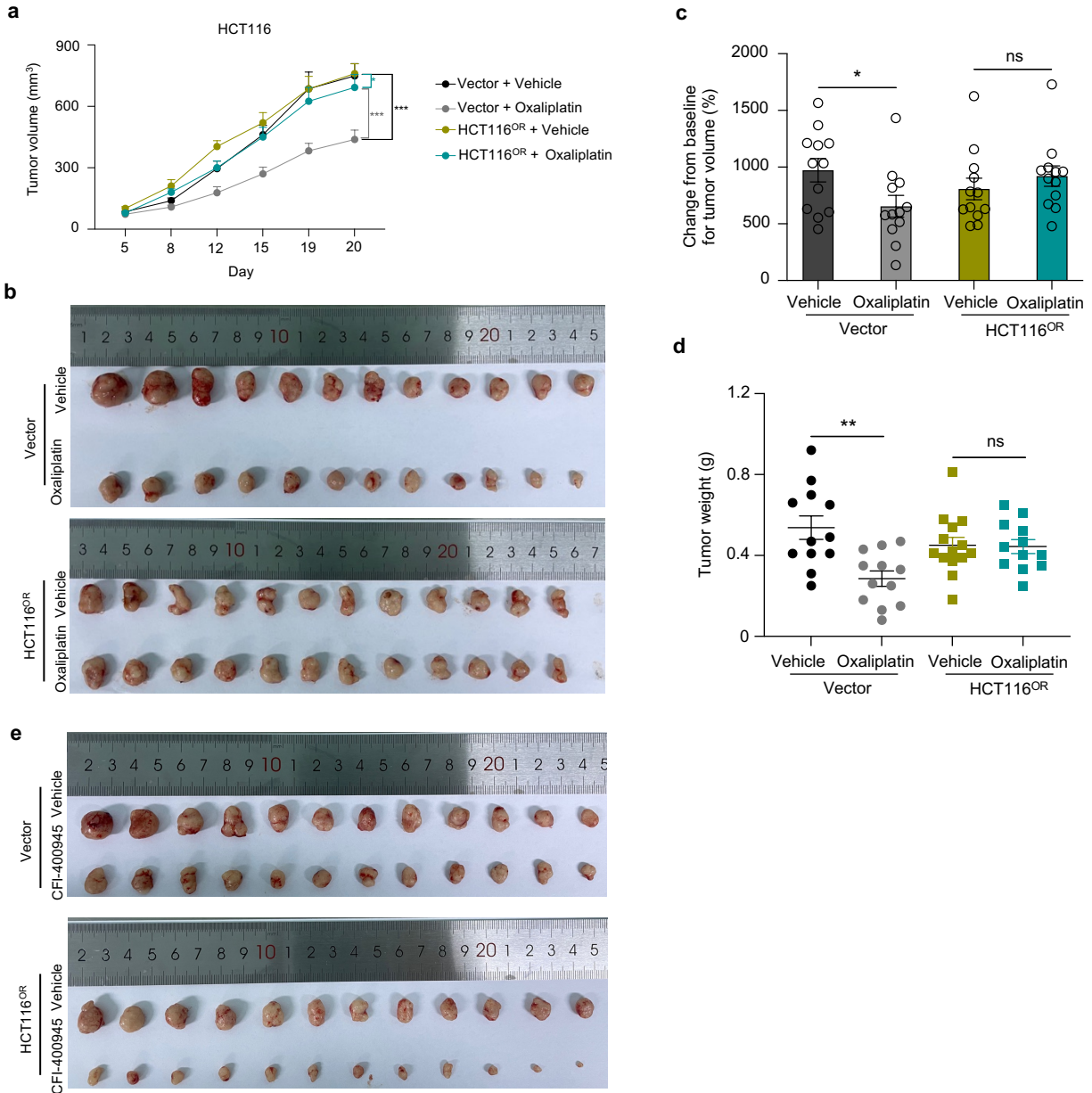
f, Apoptosis assay by PI and Annexin V staining showing that knockout of *PLK4* does not affect apoptosis of oxaliplatin-sensitive or -resistant cell lines. Mean \pm SD with n = 3 biological replicates.

g, Apoptosis assay by PI and Annexin V staining showing that CFI-400945 does not affect apoptosis of oxaliplatin-sensitive or -resistant cell lines. Mean \pm SD with n = 3 biological replicates.



Supplementary Fig. 15 | RNA-seq analysis of PLK4 target genes in oxaliplatin-sensitive or -resistant cells.

- a**, Heatmap showing *PLK4* downstream target genes of indicated oxaliplatin-sensitive (Vector) and -resistant cells determined by RNA-seq.
- b**, Venn diagram of *PLK4* target genes in four indicated cell lines.
- c**, Functional terms enriched among up-regulated *PLK4* target genes for each indicated cell line. Unpaired two-sided t test for *p* value with Benjamini-Hochberg (BH) adjustment.
- d-e**, Functional terms specifically enriched among up-regulated genes (**d**) or down-regulated genes (**e**) upon *PLK4* knockout in oxaliplatin-resistant cell lines but not in sensitive cells (Vector). Unpaired two-sided t test for *p* value with Benjamini-Hochberg (BH) adjustment.
- f**, The expression change of typical pericentriolar material (PCM) scaffolding genes upon *PLK4* knockout in each indicated cell line.



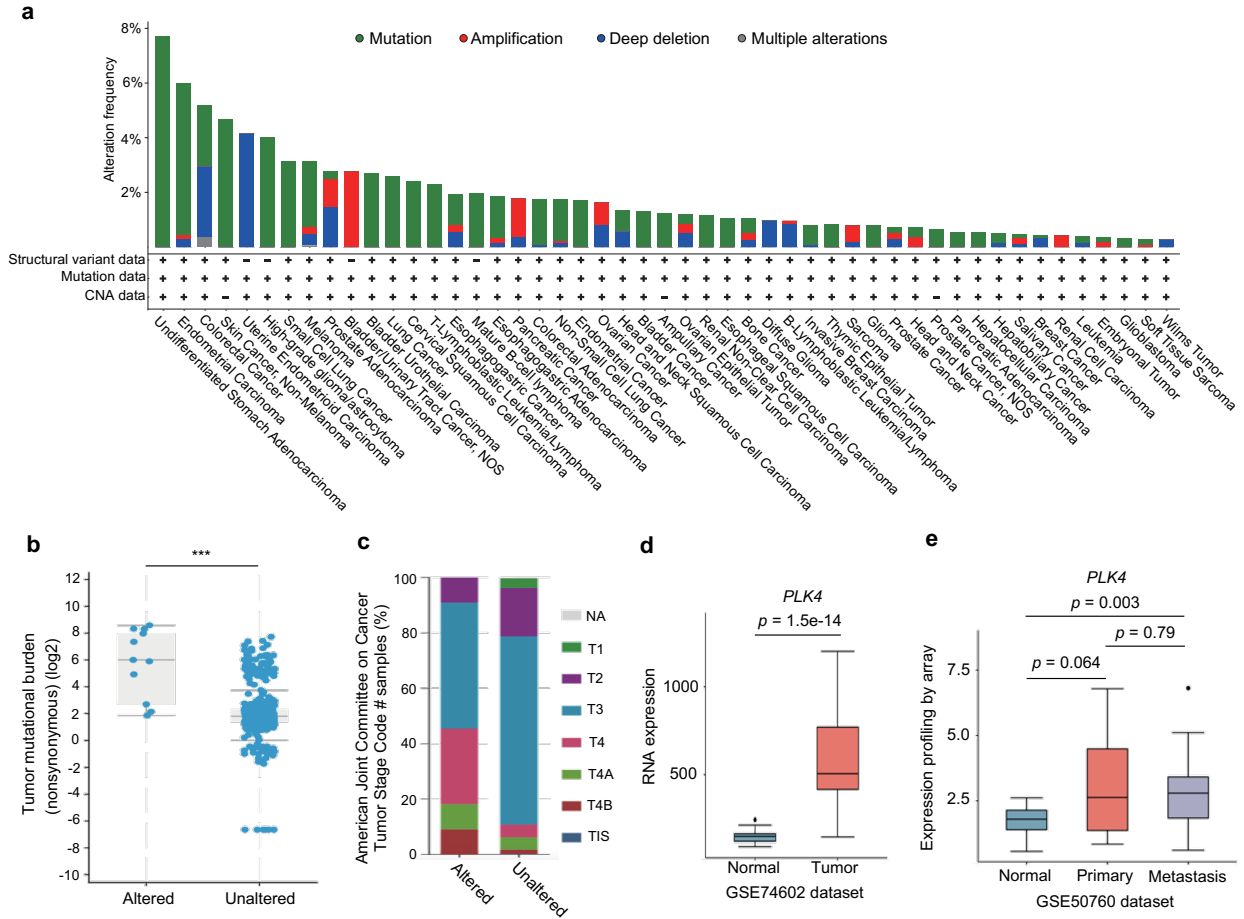
Supplementary Fig. 16 | Validation of oxaliplatin resistance by xenograft model in mice.

a, Tumor volume measured at indicated time points after xenograft implantation for oxaliplatin-sensitive (Vector) or -resistant (HCT116^{OR}) xenograft treated with vehicle or oxaliplatin. (n=12, number of tumor). Mean ± SEM. Two-way ANOVA, ****p* < 0.001.

b, Photos of tumors collected from oxaliplatin-sensitive or -resistance xenograft bearing mice with vehicle or oxaliplatin treatment at the experimental endpoint.

c-d, Relative tumor volume (compared to day 0) (**c**) or tumor weight (**d**) of mouse xenografts for indicated HCT116 cells measured at Day 20 post implantation. (n=12, number of tumor). Mean ± SEM. Unpaired two-sided t test, **p* < 0.05 and ***p* < 0.01. ns, non-significant.

e, Photos of tumors collected from oxaliplatin-sensitive or -resistance xenograft bearing mice with vehicle or CFI-400549 treatment at the experimental endpoint.



Supplementary Fig. 17 | Clinical relevance of PLK4.

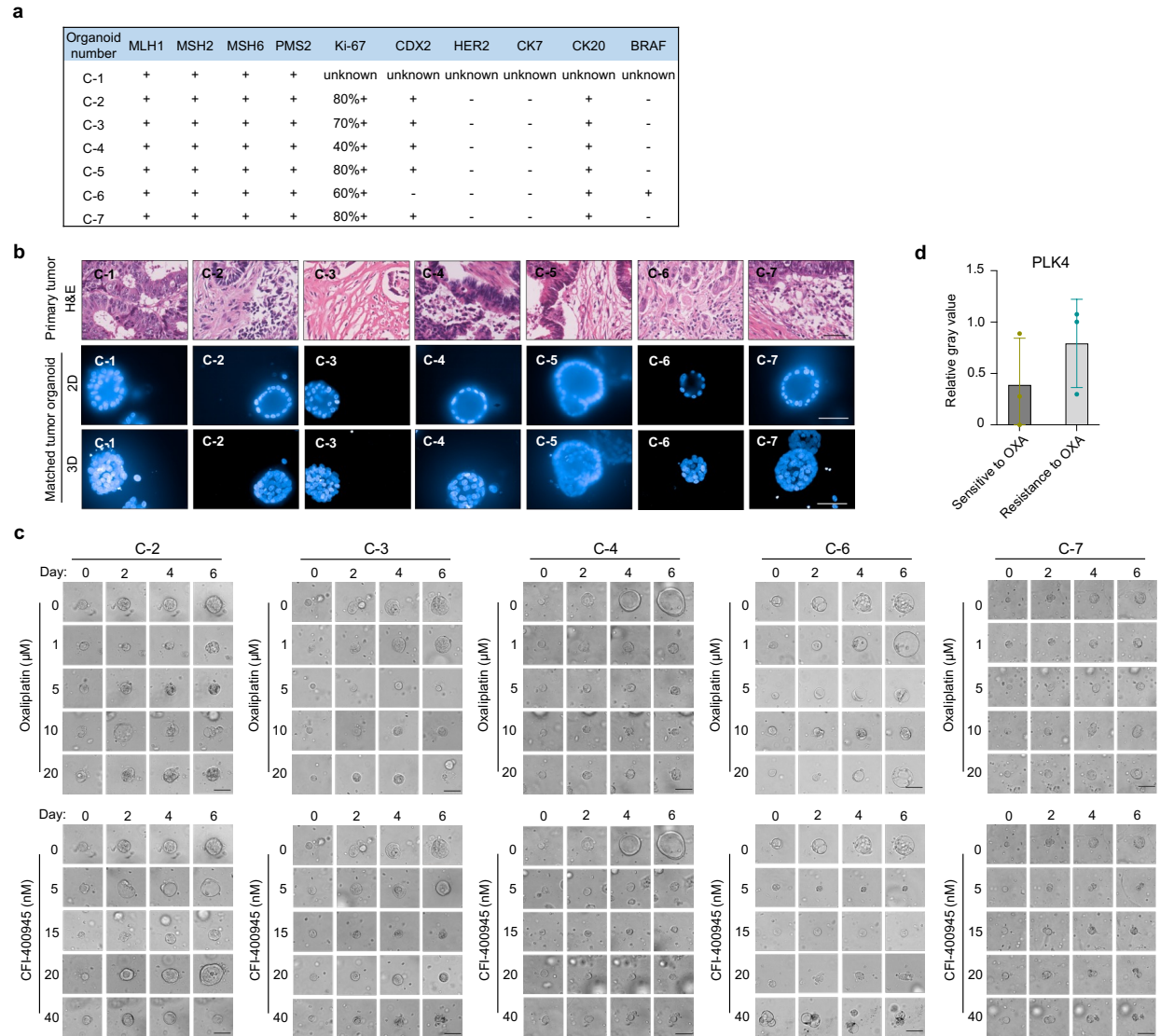
a, Overview of *PLK4* alterations across multiple cancers from cBioPortal.

b, Colorectal cancers with mutated *PLK4* tend to have significantly higher tumor mutational burden according to TCGA data from cBioPortal. Unpaired two-sided t test, $p = 8.285e-6$.

c, *PLK4* mutation is positively associated with advanced progression of colorectal cancers.

d, RNA expression of *PLK4* in GSE74602 dataset. Significance was calculated by the Wilcoxon test.

e, RNA expression of *PLK4* in GSE50760 dataset. Significance was calculated by the Wilcoxon test.



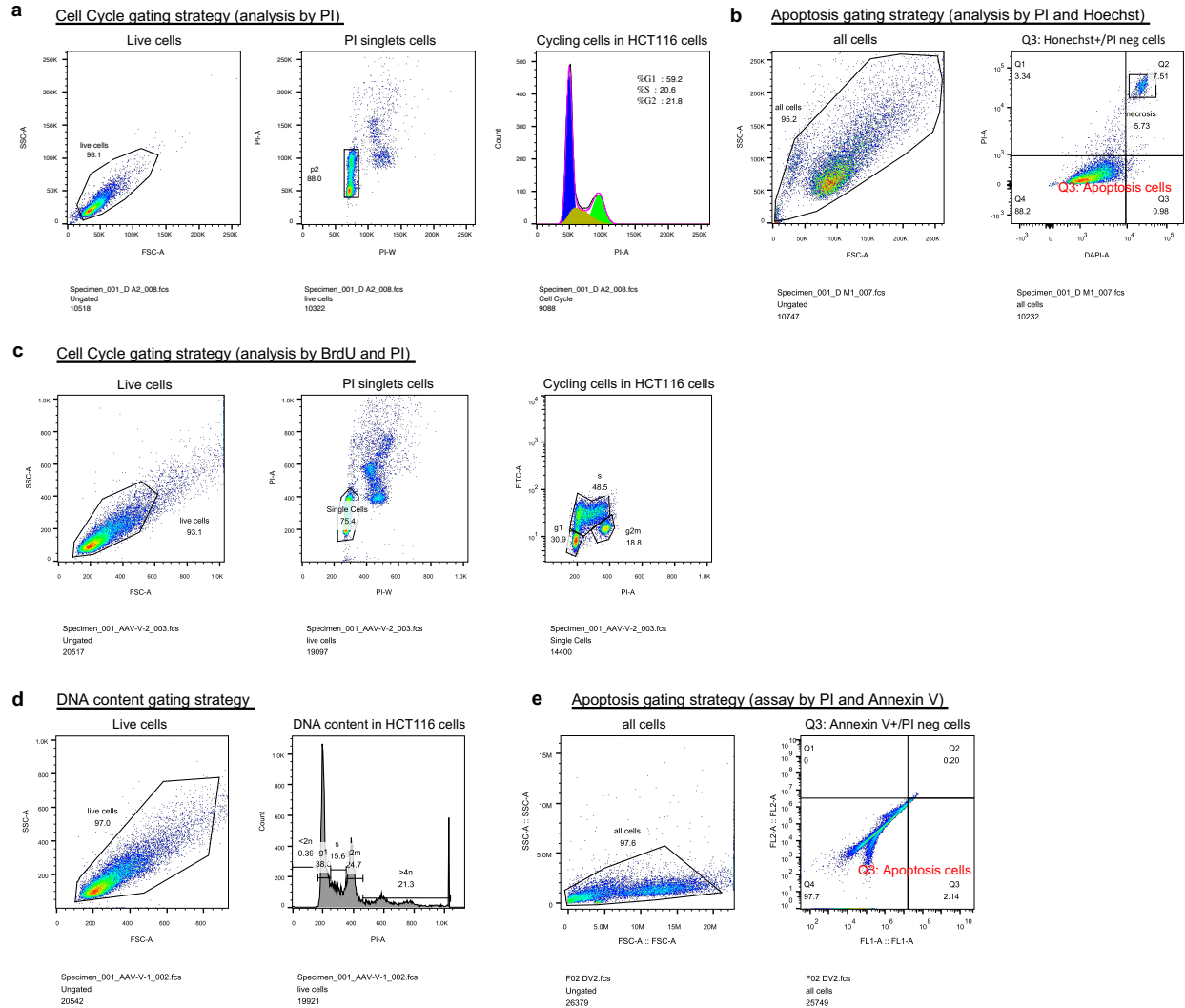
Supplementary Fig. 18 | Characterization and drug sensitivity test of patient-derived organoids.

a, Molecular characterization for several clinical biomarkers in tumors for deriving organoids.

b, Images showing H&E staining of primary tumors and Hoechst 33342-stained tumor-derived organoids. Scale bar, 50 μm .

c, Representative images showing organoid growth in response to oxaliplatin or CFI-400945 for indicated organoids. Scale bar, 50 μm .

d, Comparison of relative protein expression of PLK4 in oxaliplatin-resistant tumor tissues (C-5, C-6 and C-7) vs. in oxaliplatin-sensitive tumor tissues (C-1, C-2 and C-3) according to immunoblot image in Fig. 7d. Mean \pm SD with $n=3$ independent samples.



Supplementary Figure 19 | FACS gating strategy.

a, The gating strategy for cell cycle analysis by PI staining. Cells were first gated on SSC-Area and FSC-Area for morphology to remove debris. Doublets and cell aggregates were excluded by gating in single cells (PI-Width vs. PI-Area). The cell population gated in after debris and doublet exclusion was then used to create single-staining histograms. This gating strategy was used for Figs. 4c; S6a-b; and S7c.

b, The gating strategy for apoptosis analysis by PI and Hoechst staining. Cells were gated on SSC-Area and FSC-Area for morphology to remove debris. Cells were plotted for PI and Hoechst parameters to identify apoptosis and necrosis cells. This gating strategy was used for Figs. 4e and S7d.

c, The gating strategy for cell cycle analysis by BrdU and PI staining. Cells were gated on SSC-Area and FSC-Area for morphology to remove debris. Doublets and cell aggregates were excluded by gating in single cells (PI-Width vs. PI-Area). Cycling cells were then identified using BrdU and PI parameters in each subpopulation. This gating strategy was used for Fig. 6a-b.

d, The gating strategy for DNA content analysis. Cells were gated on SSC-Area and FSC-Area for morphology to remove debris. Cycling cells were then identified using PI parameters for DNA content analysis. This gating strategy was used for Fig. 6g-h.

e, The gating strategy for apoptosis analysis by PI and Annexin V. Cells were gated on SSC-Area and FSC-Area for morphology to remove debris. Cells were plotted for PI and Annexin V parameters to identify apoptotic cells. This gating strategy was used for Fig. S14f-g.